Metrol. Meas. Syst., Vol. XX (2013), No. 3, pp. 491–500.

PAN POLSKA AKADEMIA NAUK

METROLOGY AND MEASUREMENT SYSTEMS

Index 330930, ISSN 0860-8229

www.metrology.pg.gda.pl

M&MS

CHARACTERIZATION OF MATERIAL DEFECTS USING ACTIVE THERMOGRAPHY AND AN ARTIFICIAL NEURAL NETWORK

Sebastian Dudzik

Częstochowa University of Technology, Faculty of Electrical Engineering, Armii Krajowej 17 Ave., 42-200 Częstochowa, Poland (sebdud@el.pcz.czest.pl)

Abstract

In the paper a method using active thermography and a neural algorithm for material defect characterization is presented. Experimental investigations are conducted with the stepped heating method, so-called time-resolved infrared radiometry, for the test specimen made of a material with low thermal diffusivity. The results of the experimental investigations were used in simulations of artificial neural networks. Simulations are performed for three datasets representing three stages of the heating process occurring in the investigated sample. In this work, the simulation research aimed to determine the accuracy of defect depth estimation with the use of the mentioned algorithm is descibed.

Keywords: active thermography, non-destructive testing, defect characterization, neural networks.

1. Introduction

1.1. Defect characterization using active thermography

Non-destructive testing is applied for the detection of material discontinuity, without changing the properties of the investigated objects. This makes it possible to control the quality of products [1]. In non-destructive testing, different methods are applied: ultrasound, radiological, eddy currents and passive [2-5] and active infrared thermography procedures [6-8].

A defect localized in the subsurface material layer can be detected using thermal wave theory [9, 10]. The method based directly on this theory is called lock-in thermography, modulated thermography or phase sensitive modulated thermography. It is based on applying a periodical thermal input to the tested sample and recording, using an infrared camera, the temporal sequence of thermograms representing the instant surface temperature field of the sample. In practice, generation of the modulated thermal input is technically difficult and can be economically ineffective. In such cases, the often-used solutions are: pulsed thermography or its modifications, like pulsed-phase thermography and the stepped heating method [10-13].

Let us assume that the sample geometry consists of two material layers with different thermal properties. In such a situation the second sample layer may represent a subsurface material defect. For such a geometry, temperature evolution on the heated surface, caused by the thermal step excitation is given by the following relationship [6-8]:

$$T(\tau) = C_c \sqrt{\tau}\left\{1 + \sum_{n=1}^{\infty} 2(-\Gamma)^n \left[\exp\left(-\frac{n^2 L^2}{\alpha_0 \tau}\right) - \frac{nL\sqrt{\pi}}{\sqrt{\alpha_0 \tau}} \operatorname{erfc}\left(\frac{nL}{\sqrt{\alpha_0 \tau}}\right)\right]\right\} \text{ (K)}, \tag{1}$$

Article history: received on Oct. 14, 2011; accepted on Jun. 26, 2013; available online on Sep. 15, 2013; DOI: 10.2478/mms-2013-0042.

where:
C_c – constant related to energy absorption, Γ – mismatch factor, dependent on the effusivities of the material layers e_0 and e_1 - $\Gamma = (e_1 - e_0)/(e_1 + e_0)$, L – thickness of the surface layer (defect depth) (m), α_0 – thermal diffusivity of the surface layer, ($m^2\ s^{-1}$).

Besides, in many applications it is necessary to determine the defect parameters, such as depth, size and heat resistance. The process of quantitative determination of these parameters is called defect characterization [11-14]. The defect characterization using active thermography is a complex inverse heat transfer problem [15, 16]. Algorithms of the defect characterization can be divided into several groups:

- based on analytic approach,
- based on numerical modeling of defects (finite difference method, finite element method and other),
- based on statistical analysis of time sequences of thermal images,
- black-box methods, including methods based on neural networks and fuzzy logic,
- others.

Equation (1) is only a one-dimensional approximation of the thermal step response. Because of the lack of an accurate model, in the paper an algorithm based on the artificial neural network was proposed. For characterization of defects in a material surface layer one can apply a multi-layer feed-forward artificial neural network trained with the backpropagation algorithm. In order to use the neural network, a calibration process is necessary.

1.2. Neural algorithm for defect depth estimation

Defect depth estimation can be considered as a classification [12, 17] or regression [18] problem. In this work, the regressive neural network was applied. In such case, the neural network acts as an approximator of the solution of the inverse heat transfer problem [15]. The general scheme of the regressive algorithm uses the neural network is shown in Fig. 1.

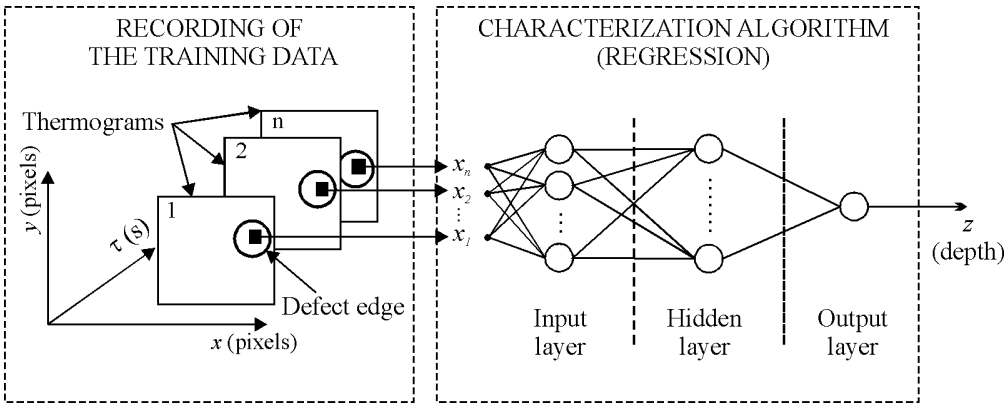

Fig. 1. Scheme for the estimation of defect depth using the multi-layer perceptron network as a regressive algorithm.

The first stage of the characterization is recording of the temporal sequence of the thermograms of the investigated surface. Next, the training vector is formed. It consists of the n temperature values assigned to a particular pixel for every time instant. The size of the input vector (the number of inputs of the neural network) is determined (but has not to be equal) by the number of the time instants (depending on the sample period). In this work the principal component analysis was employed. Therefore the number of inputs of the neural network is equal to the number of chosen components. The data preprocessing is fully described in a

later part of this paper. The number of the training vectors (samples) equals the number of pixels in the considered field of view of the investigated material surface or the number of pixels in the defective areas only. In the simulations presented in this work the second case was assumed. In a regressive network, the output layer has a single neuron. During the training, the known depth value, assigned to the given pixel, is applied to the network output. In the aforementioned characterization algorithm, the multi-layer feed-forward neural network, trained with the backpropagation routine can be used [2, 12, 19, 20].

2. Experimental investigations

2.1. Measuring stand

Experiments were performed using the measuring stand shown in Fig. 2. The measurement stand consists of the long-wave infrared camera FLIR ThermaCAM PM595 (1), digital module of communication interface (2) and a PC computer (3) capable of real-time acquisition of temporal sequences of thermograms [7, 8]. Two modeling lamps (4) of 250 W each were used as the source of thermal excitation. The examined object was a test specimen (5), made of Plexiglas. In order to isolate from adverse ambient radiation, the equipment was placed in the closed investigation chamber (6) 2,5 m x 3 m x 1,5 m (height x width x depth). The inner walls of the chamber were painted with black matt lacquer with a high value of the emissivity coefficient. The surface of the examined specimen was covered with black matt lacquer, featuring a high emissivity coefficient ($\varepsilon \approx 0{,}98$) as well. On the bottom side of the sample six non-passing holes were drilled. The six defects located at $z_1 =$ 0,8 mm, $z_2 = 1{,}0$ mm, $z_3 = 1{,}1$ mm and $z_4 = 1{,}3$ mm $z_5 = 1{,}7$ mm, $z_6 = 2{,}0$ with respect to the upper side of the sample were simulated. The sample dimensions, the location and dimensions of the holes are depicted in Fig. 3.

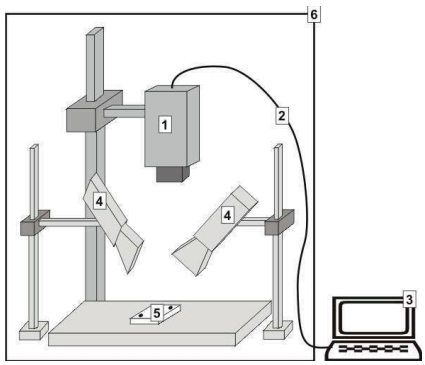

Fig. 2. Measuring stand for defect characterization using the stepped heating method.

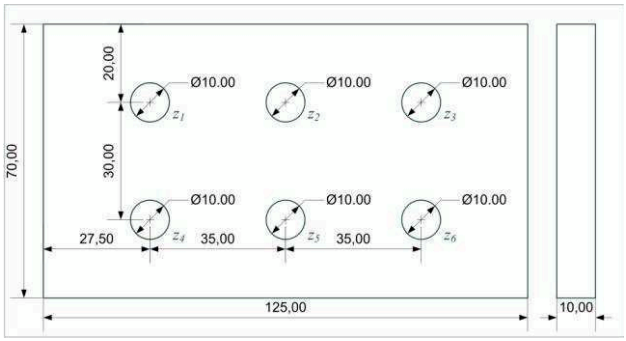

Fig. 3. Dimensions and localization of the simulated defects in the investigated specimen.

2.1. Results of the experimental investigations

In the experimental investigations the stepped heating method was used. During the experiments, the specimen surface was heated with a 500 W thermal pulse, duration time 120 s. Two lamps were used, the 250 W each. The thermogram sequence was recorded during the 120 s of the heating stage, and subsequently during 300 s of the cooling stage. The sampling frequency was set to 1 Hz, and the total number of recorded thermograms was 420. The exemplary thermograms are presented in Figs 4-7. In Figs 4, 5, thermograms for $\tau = 5$ s (early heating stage) and $\tau = 120$ s (the end of the heating stage) are depicted. Thermograms for $\tau = 270$ s (half of the observation time of the cooling stage) and for $\tau = 420$ s (the end of the cooling stage) are presented in Figs 6, 7 respectively.

3. Simulation research

3.1. Methodology of research

In this work, in order to estimate the defect depths, a neural algorithm based on the regressive neural network was used. The simulations were performed in the following stages:

1. Selection of the training data.
2. Principal component analysis (PCA).
3. Selection of the neural network architecture.
4. Training the neural network with the backpropagation training algorithm.
5. Testing of trained network using the cross-validation procedure.
6. Analysis of the simulation results.

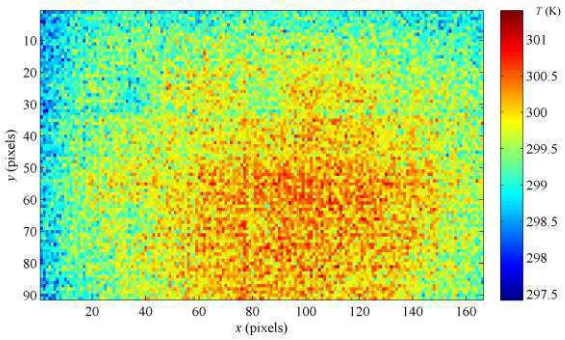

Fig. 4. Thermogram of investigated sample for $\tau = 5$ s.

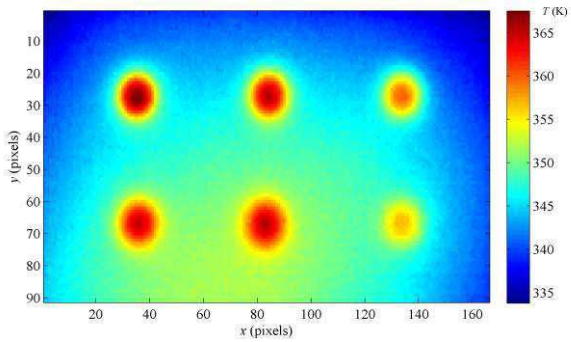

Fig. 5. Thermogram of investigated sample for $\tau = 120$. s.

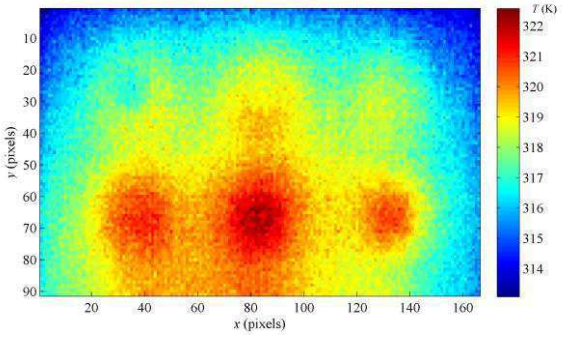

Fig. 6. Thermogram of investigated sample for $\tau = 270$ s.

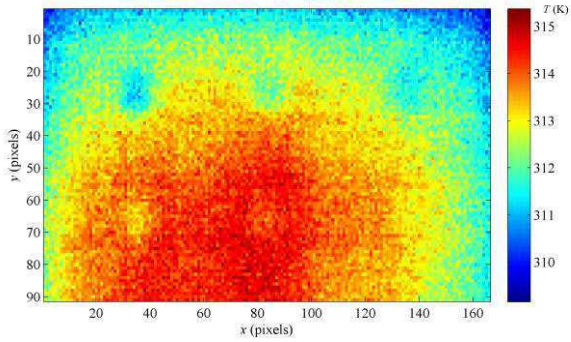

Fig. 7. Thermogram of investigated sample for $\tau = 420$ s.

The simulation research was performed on data obtained from the temporal thermogram sequences, recorded in experiments described in Section 2. As the basis of the analysis, the three sequences of thermograms, recorded for heating phase going to120 s, cooling phase going to 300 s and both phases lasting totally for 420 s were used. For each sequence the following number of features was established: 120 for the heating phase, 300 the for cooling phase and 420 for both phases. In order to limit the inputs of the neural network, in simulations the principal component analysis (PCA) was utilized. The PCA is a statistical procedure enabling the transformation of object features [21]. As the result of this transformation, the description of the object features in a new space is obtained. Each new component is a linear combination of the original features, computed so that the variance would be maximized. Subsequent components are determined taking into account the orthogonality criterion [22]. As a result of transformation, a new set of features is obtained. These are sorted in the variance descending order. In order to fix the number of principal components, the criterion based on the percentage of variance explained was used. If the sum of the variance of the given number of components is the significant part of the variance of all components, it means that these components explain the original data variance well enough. In this paper, the optimal number of components for which the cumulated sum of the variance explained equals 98% was chosen. On the basis of the principal components analysis, three data sets were created. The description of the data sets used in simulations performed here is presented in Table 1.

Table 1. Description of datasets and architectures of neural networks used in simulations.

NAME	PROCESS PHASE (TIME)	NUMBER OF PRINCIPAL COMPONENTS	ARCHITECTURE OF NEURAL NETWORK
D-1	Heating (120 s)	4	4 – 16 – 1
D-2	Cooling (300 s)	3	3 – 21 – 1
D-3	Heating + Cooling (420 s)	4	4 – 16 – 1

The sample area visualized on a single thermogram measured 166×91 pixels. In paper [18] all pixels in the field of view of the thermogram were used in the network training. In this work only the pixels belonging to the defect areas were used. Such an approach enabled a more reliable assessment of the depth estimation error without the error component dependent on the detection efficiency. In the training of the considered neural network it was necessary to prepare a map of defect depths for the investigated sample. This map was made according to the scheme from Fig. 3. The map is presented in Fig. 8.

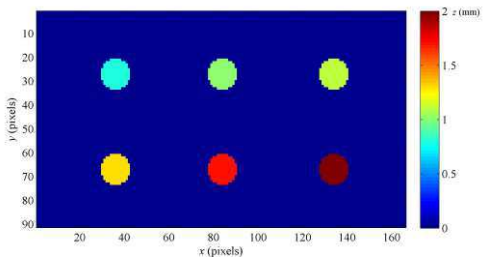

Fig. 8. The map of defect depths used for training of neural networks under investigation.

An important stage of the model creation is a selection of its structure and number of its parameters. In case of an artificial neural network, the model is constructed with the determination of neural network architecture. In this work, the feed-forward neural network with one hidden layer, so-called multi-layer perceptron, was examined [11, 18]. One of the

stages of network design is the selection of number of neurons in the hidden layer. In simulations it was assumed that the number of neurons in the hidden layer depends on the number of training samples. Moreover, it was stated that for proper generalization, the number of weights would be ten times lower than the number of the training samples. On the basis of the aforementioned rule, taking into account the number of inputs, the number of neurons in hidden layers was fixed. In simulations many neural networks with different architectures were examined. The numbers of hidden neurons presented in Table 1 were fixed in the 10-fold cross-validation procedure described below. These numbers correspond to the networks for which the smallest errors defined by formula (5) were obtained. The number of neurons in the input layer resulted from the size of the input data vector. It was fixed depending on the dataset (see: Table 1). Finally, the output layer of the considered network had a single neuron. The neural network architectures assumed for every dataset are presented in Table 1 (shown in the last column). Individual numbers denote respectively: the number of inputs, the number of neurons in the hidden layer and the number of neurons in the output layer.

The main purpose for the supervised neural network training is the minimization of difference between the known output and the output of the considered network. The most frequently used error criterion is the mean squared error. However, a very important feature of the neural network is its generalization ability. Thanks to it, the network trained with the training data is able to generate correct results for the testng data, which did not take part in the training process.

In order to derive the generalization error in this work, the 10-fold cross-validation procedure of the given neural networks was applied. The set of all available samples (pixels belonging to the defect areas) S_{all} were randomly divided into the 10 equinumerous subsets $S_{test}(i)$, $i = 1, \ldots, 10$. At the i-th iteration, training of the network with the (S_{all}-$S_{test}(i)$) set was performed. Then the network was tested using the set $S_{test}(i)$ and the error for testing data was calculated. Finally, the network output, as the map of defects' depths for the considered field of view was formed.

The last stage of the simulation research was the analysis of the results and evaluation of the defect depth estimation accuracy. In this work, the following criteria for accuracy evaluation were assumed:

- The mean error of depth estimation in the defect area, for training data:

$$\Delta z_{LEARN} = \frac{1}{N_{def}} \sum_{i=1}^{N_{def}} \left| z_{LEARN}(i) - z_R \right| \text{ (mm)}, \tag{2}$$

  where: N_{def} – number of pixels in the defect area, $z_{LEARN}(i)$ – depth of defect assumed for i-th pixel in the field of view, calculated by the neural network for training data, z_R – correct (real) value of defect depth, applied in the training to the output of network.
- The relative mean error of depth estimation in the defected area, for training data:

$$\delta_{Z-LEARN} = \frac{\Delta z_{LEARN}}{z_R} \text{ (\%)}. \tag{3}$$

- The mean error of depth estimation in the defect area, for testing data:

$$\Delta z_{TEST} = \frac{1}{N_{def}} \sum_{i=1}^{N_{def}} \left| z_{TEST}(i) - z_R \right| \text{ (mm)}, \tag{4}$$

  where: $z_{TEST}(i)$ – depth of defect assumed for i-th pixel in the field of view, calculated by the neural network for testing data.
- The relative mean error of depth estimation in the defected area, for testing data:

$$\delta_{Z-TEST} = \frac{\Delta z_{TEST}}{z_R} \text{ (\%)}. \tag{5}$$

Besides determination of the errors expressed with formulas (2-5), in this paper a regression analysis was performed. During the analysis, the linear correlation coefficients between the correct depth values and the values obtained using the neural network, for training and testing data, were calculated. Furthermore, the coefficients of the linear regression were derived. These coefficients and the linear equations are shown in Figs 11, 14, 17.

3.2. Simulation results

Simulations of the aforementioned neural algorithm for defect characterization were performed in accordance with the methodology described in the preceding section. The results for dataset D-1, obtained with the cross-validation routine were shown in Figs 9-11. In Fig. 9 the results of neural network simulation for testing data were presented. The relative mean errors, for the particular defect depths z, defined by equation (5), were depicted in Fig. 10. The results of the regression analysis obtained with the considered dataset for testing data, are presented in Fig. 11.

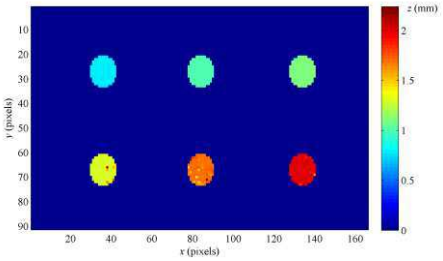

Fig. 9. The map of defects' depth obtained for testing data (D-1).

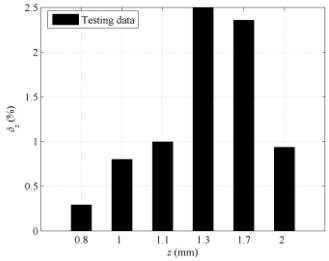

Fig. 10. The relative mean errors defined with (5), obtained for testing data (D-1).

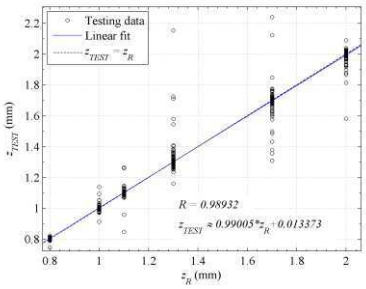

Fig. 11. Results of the regression analysis, obtained for testing data (D-1).

In Figs 12-14, the simulation results for dataset D-2 were presented. The results of the neural network simulations for testing data were depicted in Fig. 12. The relative mean errors defined by formula (5) were shown in Fig. 13. In Fig. 14 the results of the regression analysis were presented.

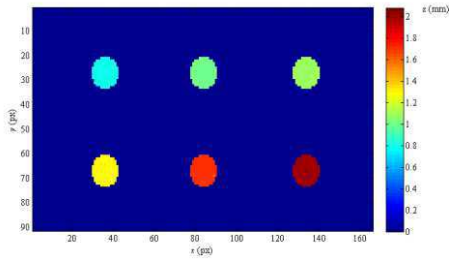

Fig. 12. The map of defects' depth obtained for testing data (D-2).

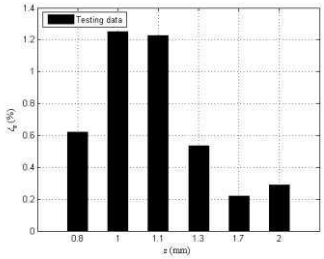

Fig. 13. The relative mean errors defined by (5), obtained for testing data (D-2).

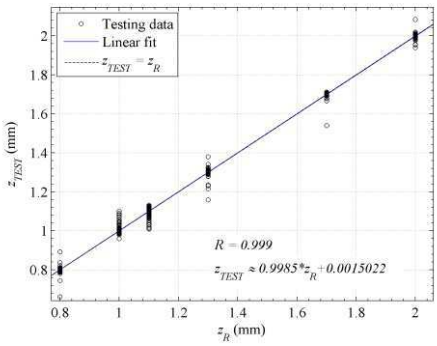

Fig. 14. Results of the regression analysis, obtained for testing data (D-2).

The results for dataset D-3, obtained with the cross-validation routine are shown in Figs 15-17. In Fig. 15 the results of neural network simulation for testing data are presented. The relative mean errors, for the particular defect depths z, defined by equation (5), are depicted in Fig. 16. The results of the regression analysis obtained with the considered dataset for testing data, are presented in Fig. 17.

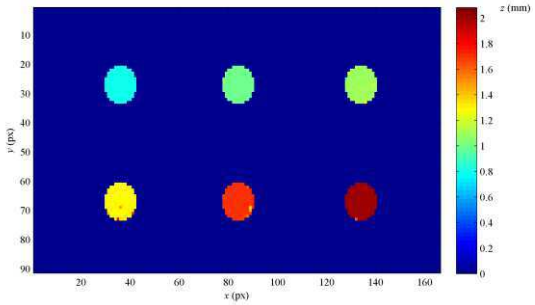

Fig. 15. The map of defects' depth obtained for testing data (D-3).

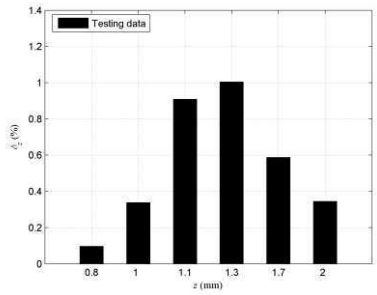

Fig. 16. The relative mean errors defined with (5), obtained for testing data (D-3).

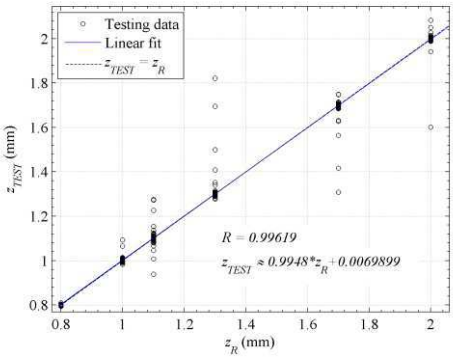

Fig. 17. Results of the regression analysis, obtained for testing data (D-2).

4. Conclusions

In this paper, the results of the experimental and simulation investigations of a neural algorithm for defect characterization were presented. Analyzing the results of experimental tests, the following conclusions may be drawn:

- In the experimental investigations conducted in this work, the maximum thermal contrast for the particular defects was observed at the end of the heating phase

(τ = 120 s) – cf. Fig. 5. It follows that the visibility of a defect is strictly depending on the time instant of observation and defect depth – cf. Fig. 5, 6.

- Taking into account the abovementioned issue, it is difficult to establish the time instant for the maximum thermal contrast, only on the basis of the thermal parameters of investigated material and the heat input properties, using equation (1).

Analyzing the results of simulation tests, the following conclusions have been formulated:

- The application of the principal components analysis (PCA) allowed a significant limitation of the size of input data vectors used for training of the investigated neural networks. Decreasing the size of input data vectors allowed decreasing the total number of weights. It enabled significantly a decrease of the accuracy of defect depth estimation, especially for testing data.
- Comparing the maps of defects' depth, formed using the neural network response, for testing data, it can be stated that these are similar to the map of defects' depths used for training of neural networks, for every dataset D-1, D-2, D-3 – cf. Figs 8, 9, 12, 15.
- The above remark was confirmed by a quantity analysis performed with the use of relative mean errors in the defect areas, defined with the use of formula (5) – cf. Figs 10, 13, 16.
- The biggest values of the relative error of depth estimation were noticed for dataset D-1 (i.e. for thermograms' sequence recorded for the heating stage). The smallest values of error described by equation (5) occurred for dataset D-3 (i.e. for thermograms' sequence recorded for both stages of the considered heat transfer process).
- Comparing the values of errors for datasets D-2 and D-3, it can be stated that they are not significantly different – cf. Figs 13, 16. Taking into account the abovementioned conclusion, it can be formulated that limiting the recording time of the thermogram sequence in the experimental investigations does not significantly reduce the characterization accuracy with the method described here, especially when the cooling stage instead of the heating and cooling stages will be recorded. It is necessary to emphasize that this conclusion is strictly related to experiments prepared in the present work with the use of the stepped heating method and a sample made of a material with a low thermal diffusivity value.
- Good statistical agreement between the network output and the real depth values, for the testing data, is confirmed by the results of the regression analysis – cf. Figs 11, 14, 17. For all three examined datasets, it was noticed that a high value of the correlation coefficient R occurred between the neural network output depth values and the values of depth applied in the training process – cf. Figs 11, 14, 17.
- The method presented in this paper can be applied after prior detection of a defect. The main purpose of this work was to present the results of research on the data processing algorithm, not a method ready to be deployed. However, the accuracy of the mentioned algorithm appears to be satisfactory. The method is designed so that the neural networks should be trained in the laboratory and the depth estimation should be conducted at the production line. However, there are many problems related to practical use of this method (e.g. eliminating the uneven heating).
- It should be emphasized that the results obtained in this work are valid for the defect's depth ranging from 0,8 to 2 mm, the aerial defects and the materials with low thermal diffusivity close to thermal diffusivity of Plexiglas (i.e. 0,12 x 10^{-6} m^2 s^{-1}) which has been used in the tests.

References

[1] Lewińska-Romicka A. (2001). *Nondestructive Testing. Fundamentals of Defectoscopy*. Warsaw: Scientific and Technical Publishers.

[2] Dudzik S. (2011). Investigations of a heat exchanger using infrared thermography and artificial neural networks. *Sensors & Actuators: A. Physical*, 166 (1), 149-156.

[3] Madura H. (2004). *Thermovision measurements in practice.* Warsaw: Measurement, Automation, Control Publishers (edited by Madura H.).

[4] Minkina W. *Thermovision Measurements – Instruments and Methods*. Częstochowa: Publishing Office of Częstochowa University of Technology.

[5] Minkina W., Dudzik S. (2009). *Infrared Thermography – Errors and Uncertainties*. Chichester: J. Wiley & Sons.

[6] Maldague X.P. (2001). *Theory and Practice of Infrared Technology for Nondestructive Testing*. New York: J. Wiley & Sons Interscience.

[7] Dudzik S. (2009). A simple method for defect area detection using active thermography. *Opto-Electronics Review*, 17 (4), 338-344.

[8] Dudzik S. (2010). Approximation of thermal background applied to defect detection using the methods of active thermography. *Metrology and Measurement Systems*, 17 (4), 621-636.

[9] Fourier J. (1826). Théorie du mouvement de la chaleur dans les corps solides-2 Partie. *Mémoires de l' Academie des Sciences*, 153 (5), 185-555.

[10] Maldague X., Galmiche F., Ziadi A. (2002). Advances in pulsed phase thermography. *Infrared Physics & Technology*, 43, 175-181.

[11] Gleiter A., Spiessberger C., Busse G. (2008). Phase angle thermography for depth resolved characterization. In *Proceedings of 9th International Conference on Quantitative Infrared Thermography QiRT'08*. Cracow, Poland, 435-441.

[12] Vallerand S., Maldague X. (2000). Defect characterization in pulsed thermography: a statistical method compared with Kohonen and Perceptron neural networks. *NDT&E International* 33, 307–315.

[13] Zöcke C., Langmeier A., Stöβbel R., Arnold W. (2009). Reconstruction of the defect shape from lock-in thermography phase images. *QIRT Journal,* 6 (1), 63-78.

[14] Avdelidis N.P., Hawtin B.C., Almond D.P. (2003). Transient thermography in the assessment of defects of aircraft composites. *NDT&E International*, 36, 433-439.

[15] Alifanow O.M. (1994). *Inverse Heat Transfer Problems.* Berlin Heidelberg: Springer-Verlag.

[16] Kreith F. (2000). *The CRC Handbook of Thermal Engineering*. CRC Press, LLC.

[17] Benitez H.D., Loaiza H., Caicedo E., Ibarra-Castanedo C., Bendada A., Maldague X.P. (2009). Defect characterization in infrared non-destructive testing with learning machines. *NDT&E International*, 42, 630-643.

[18] Dudzik S., Minkina W. Analysis of the accuracy in determination of defect depth using an active infrared thermography and artificial neural network. In *Proceedings of 43th Inter−University Conf. of Metrologists MKM'11*. Invited paper, 289-307.

[19] Li H., Chen C.L.P. (2001). *Fuzzy Neural Intelligent Systems. Mathematical Foundation and the Applications in Engineering*. CRC Press, LLC.

[20] Osowski S. (2000). *Neural networks applied to the processing of information*. Warsaw: Publishing Office of the Warsaw University of Technology.

[21] Michie D., Spiegelhalter D.J., Taylor C.C. (1994). *Machine Learning, Neural and Statistical Classification*. Prentice Hall.

[22] Fukunaga K. (1990). *Introduction to Statistical Pattern Recognition*. Academic Press 1990 2nd ed.